DOMAIN WALL FERMIONS IN VECTOR THEORIES

PAVLOS M. VRANAS
Physics Department
University of Illinois
Urbana, IL 61801, USA
vranas@uiuc.edu

Abstract. Applications of Domain Wall fermions to various vector-like lattice theories are reviewed with an emphasis on QCD thermodynamics. Methods for improving their chiral properties at strong coupling are discussed and results from implementing them are presented.

1. Introduction

Domain Wall fermions (DWF) provide an alternative to traditional lattice fermion methods. Since their introduction to lattice field theory [1, 2] they have produced a wealth of theoretical and numerical advances for vector and chiral lattice theories (see [3] and references therein; also see these proceedings [4, 5, 6]).

DWF are defined in a space-time with an extra dimension. A mass defect along the extra direction causes one chirality of the Dirac spinor to get exponentially localized along the defect. If the extra direction is finite an anti-defect will necessarily be present and the other chirality will also get exponentially localized. As a result, the two chiralities of a Dirac spinor have been separated and their mixing is only exponentially small. This is suitable to vector-like theories. The effects of the defect, anti-defect can also be produced if the theory is defined without them, but the boundary conditions along the extra direction are free [7, 8]. Then each chirality gets localized along a different boundary (wall). If the number of sites along the extra direction "s" is L_s then the mixing of the two chiralities is exponentially small in L_s. At $L_s = \infty$ the theory has exact chiral symmetry.

These properties make DWF a powerful tool for numerical studies that require very good control over the chiral properties. Consider dynamical

QCD thermodynamics as an example. At finite lattice spacing "a" traditional fermions (staggered or Wilson) break the chiral symmetry explicitly. The symmetry is recovered together with the Lorentz symmetry as the lattice spacing tends to zero. But the computational cost for reducing the lattice spacing is very large. Typically, in order to reduce the lattice spacing by a factor of two, one has to perform 2^{8-10} more computations (the exponent accounts for the 2^4 more lattice sites and the various algorithmic costs). On the other hand, DWF can approach the chiral limit even at finite lattice spacing by simply increasing L_s. For the first time the chiral and Lorentz symmetry limits have been separated! Furthermore the computational cost for increasing L_s is only linear in L_s making this method very appealing. Now one has control in deciding which limit to get closer to. If the interest is in the order and properties of the finite temperature phase transition one would want to bring the theory as close as possible to the chiral limit and be less concerned with the amount of Lorentz symmetry present. Of course, other applications may have different requirements.

In this work the action and numerical methods are as in [8] with the modification as in [9]. The only notation the reader will need, to follow the results presented here, is: L_s is the number of sites along the extra direction "s", m_0 is the five dimensional defect mass or domain wall "height", m_f is an explicit mass that mixes the plus chiral component localized on one wall with the minus component localized in the other wall. If $L_s = \infty$ the bare fermion mass is proportional to m_f. To put these parameters into perspective, recall that in free theory at finite L_s the effective mass is [9]:

$$m_{\text{eff}} = m_0(2 - m_0)\left[m_f + (1 - m_0)^{L_s}\right], \quad 0 < m_0 < 2 \qquad (1)$$

The exponentially small "residual" mass $m_{\text{res}} = m_0(2 - m_0)(1 - m_0)^{L_s}$ is a finite L_s effect reflecting the residual mixing of the chiral components. The range of m_0 determines the number of flavors. For $m_0 < 0$ zero flavors, $0 < m_0 < 2$ one, $2 < m_0 < 4$ four, $4 < m_0 < 6$ six, $6 < m_0 < 8$ four, $8 < m_0 < 10$ one, and $10 < m_0$ zero flavors.

A very important aspect of DWF has to do with their exceptional zero mode properties in the background of topologically non-trivial gauge fields. Sadly, this is also the reason for many of the difficulties that arise in their use. Gauge fields are introduced in the standard fashion in ordinary space-time. They do not have an extra component and they are the same across the extra direction [2, 10]. From this point of view, the extra direction can be thought of as an internal flavor space. This is the basis of the overlap formalism [10, 11]. One can see that the transfer matrix T along the extra direction is the same at every "s" slice. As a result, the effect along the extra direction is simply T^{L_s}, which at $L_s = \infty$ is a projection operator on the

ground state of the corresponding Hamiltonian H. Therefore, the fermion determinant in the background of the gauge field will be the overlap of this ground state with the state at the boundary. The state at the boundary has a fixed "filling" independent of the gauge field background. In the presence of a topologically trivial gauge field background the ground state of H has the same "filling" and the overlap of the two states is not zero. However, the filling level of the ground state of H can change depending on the background field. If this happens the overlap with the boundary state is exactly zero indicating the presence of exact zero modes. The difference of the two filling levels is an index for this operator. For smooth topologically non-trivial backgrounds it has been shown that the index theorem is satisfied [11]. Now one can see how this exceptional property is also the source of problems at finite L_s. If a background gauge field is slowly changed from one sector to another the number of negative eigenvalues of H will have to change by one. Therefore, one of the eigenvalues will have to cross zero. When this happens, the transfer matrix will have eigenvalue equal to one and there will be no decay along the extra direction and therefore no localization. The measure of such "topology changing" configurations is zero [11, 8] so the $L_s = \infty$ limit is well defined. However, configurations in their vicinity will cause very slow decay rates [12]. The effect of these configurations in numerical simulations is problematic. In order to achieve desired levels of chiral symmetry, large L_s may be needed depending on the value of the coupling constant.

In this work several applications of DWF to vector theories are presented. Also, some attempts to improve the chiral properties of DWF so that smaller L_s values can be used in numerical simulations are described. The collection of results is not intended as a summary of the whole field and only reflects the involvement of the author in the subject.

2. Schwinger model

In this section the two flavor Schwinger model is studied using DWF. This work has appeared in [9].

Before DWF could be used for QCD simulations some basic questions regarding their properties had to be investigated: (1) In the interacting theory, is the approach to the chiral limit exponential in L_s? (2) How does the exponential "decay" rate depend on the lattice spacing? (3) How large should L_s be? (4) Are anomalous effects reproduced?

The two flavor Schwinger model provides a good testing ground for these questions. It is an interacting gauge theory in which the $U_A(1)$ symmetry is anomalously broken. The corresponding t' Hooft vertex $w = [\overline{\Psi}_R \Psi_L]^2 + [\overline{\Psi}_L \Psi_R]^2$ is expected to acquire a non-zero VEV at the mass-less limit.

Furthermore, since there is no spontaneous chiral symmetry breaking, the chiral condensate can serve as a direct probe of chiral symmetry breaking due to the DWF regulator.
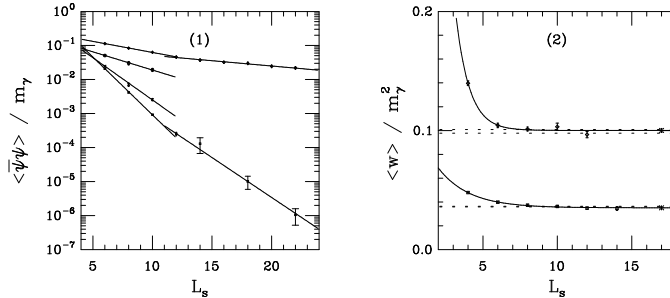
Figure 1. $\langle \overline{\Psi}\Psi \rangle$ in units of the photon mass m_γ, vs. L_s for $m_f = 0$, fixed physical volume and $m_0 = 0.9$. From top to bottom the lattice spacing is $a \sim 1/L$, with $L = 6, 8, 10, 12$.

Figure 2. $<w>/m_\gamma^2$ vs. L_s for $L = 4$ (squares) and $L = 10$ (diamonds) at $m_0 = 0.9$. The physical volume and mass are fixed.

The amount of breaking as a function of L_s and the lattice spacing "a" as "seen" by the chiral condensate $\langle \overline{\Psi}\Psi \rangle$ is shown in figure 1 for zero m_f. One can see that $\langle \overline{\Psi}\Psi \rangle$ tends to zero exponentially fast. There are two rates of decay with an inflection around $L_s = 10$. These two rates have been identified in [9] with two separate but related mechanisms. The fast decay can be thought of as being the free theory decay in the presence of small fluctuations. For example, one can imagine that in the presence of small fluctuations m_0 in eq. 1 will fluctuate and therefore even if $m_0 = 1$ the decay rate will be finite. The slower decay rate was identified with topology changing configurations of the type described in the introduction. It must be pointed out that the L_s dependence of $\langle \overline{\Psi}\Psi \rangle$ involves many different exponential decay rates. The two decay rates in figure 1 may in fact be a superposition of several exponentials. However, it is apparent that there are two different mechanisms at play and that within the error bars are nicely summarized by only two exponentials.

The next crucial observation is that the decay rates become faster as the lattice spacing is reduced. This is very important. If this was not so then numerical applications of DWF would not be appealing.

In practical applications of DWF one works at non zero m_f. If in a given application extrapolations make sense then for each value of m_f one measures at several values of L_s and extrapolates to $L_s = \infty$ using a function of the form $A + Be^{-cL_s}$. As an example, consider a measurement of w. In figure 2, w is measured vs. L_s for a non-zero mass and fitted to the above form. The extrapolated value agrees well with the value obtained using the

overlap formalism ($L_s = \infty$ limit of DWF, dotted lines). Since the overlap has been found to reproduce a non zero VEV for w at $m_f = 0$ [13, 9], one can conclude that DWF correctly reproduces anomalous effects.

3. Fermion scalar interactions

In this section the interaction of DWF with scalar particles is discussed. This work has appeared in [14].

   As discussed in the introduction, the interaction of DWF with gauge fields was treated by viewing the extra direction as an internal flavor space. Naively one would think that the interaction of DWF with a spin zero field could also be treated in the same way. This would imply an interaction of the form $\sum_s \overline{\Psi}(x,s)\sigma(x)\Psi(x,s)$. One can see that σ will play a role similar to m_0. Since the value of m_0 controls the number of flavors in the theory this is clearly the wrong way to couple the spin zero field. Instead, it should be coupled to the light degrees of freedom that "reside" on the boundaries very much like the mass term m_f:

$$\overline{\Psi}_R(x,0)\sigma(x)\Psi_L(x,L_s-1) + \overline{\Psi}_L(x,L_s-1)\sigma(x)\Psi_R(x,0) \qquad (2)$$

Therefore, it is not natural to think of the extra direction as an internal flavor space. This reveals some richness in the way different spin particles interact with DWF. In fact, the outline of some more "geometrical picture" seems to emerge.
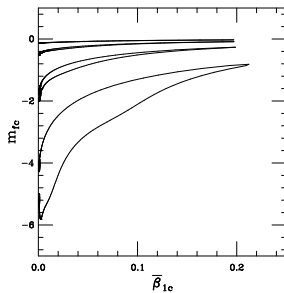
Figure 3. The large N phase boundary of the parity-flavor broken phase of the $SU(2) \times SU(2)$ four-Fermi model on a 6^3 lattice with $m_0 = 1$. From bottom to top, the L_s values are 2, 3, 4, and 5. The parity-flavor symmetry is broken inside the oval-looking regions.

   Using this type of interaction, four-Fermi and Yukawa type models can be studied with DWF. A simple $Z_2 \times Z_2$ model was studied using large N and numerical techniques. An interesting result from this study was that the minimum decay rate of these models as predicted from large N is $-ln(2 -$

$\sqrt{2}) = 0.535$. This was also confirmed numerically. A similar result has been obtained in [5].

A large N study of the $SU(2) \times SU(2)$ four-Fermi model with DWF revealed a rich small L_s structure. For small L_s and negative m_f a parity–flavor broken phase exists. This phase is of the same nature as the Aoki [15] phase of Wilson fermions. This phase was later observed in quenched QCD with DWF [16]. The large N phase boundary is shown in figure 3 (where $\bar{\beta}_1$ is proportional to the inverse of the 4-fermi coupling).

4. Zero modes for classical topological backgrounds

In this section the zero mode properties of DWF are studied in the presence of classical instanton backgrounds. This work has appeared in [17].

In the introduction it was described how at $m_f = 0$ and at the $L_s = \infty$ limit DWF can have exact and robust zero modes. This property is strictly true only at that limit. In practice, one would like to work at small but finite m_f. It is therefore natural to ask if the zero mode effects at the small m_f of interest can be reproduced for reasonable values of L_s and if these effects are stable under perturbations.
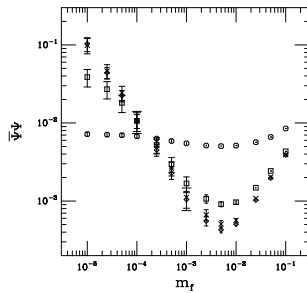
Figure 4. $\overline{\Psi}\Psi$ vs. m_f in the background of a classical instanton where random noise has been superimposed with amplitude $\zeta = 0.1$. The lattice size is 16^4. The circles, squares, crosses, and diamonds correspond to $L_s = 4, 6, 8, 10$.

This question can be addressed by studying the DWF chiral condensate $\overline{\Psi}\Psi$ as a function of m_f in the presence of a background classical instanton field with some amount of superimposed random noise with amplitude ζ. If the zero mode effects are present and are robust under fluctuations then the chiral condensate should diverge as $1/m_f$. Indeed, this is the case as can be seen from figure 4 where $\zeta = 0.1$. For $L_s = 4$ the divergence is not visible, for $L_s = 6$ it continues down to $m_f \approx 10^{-4}$ and then it "flattens out" indicating finite L_s effects. For $L_s = 8, 10$ the divergence continues down to $m_f \approx 10^{-5}$. Typical applications do not require m_f below 10^{-3}.

This result is in sharp contrast with Wilson or staggered fermions that do not have robust zero modes.

5. Quenched QCD above the finite temperature transition

In this section the effects of zero modes are studied for backgrounds that involve quantum-noise, namely backgrounds generated using the pure gauge action above the transition (quenched QCD). This has appeared in [18, 19]

In a quenched QCD simulation the zero modes are not suppressed by the fermion determinant. If the simulation is done above the finite temperature phase transition then one would expect that the chiral condensate at small masses will not vanish but instead it will diverge as $1/m_f$. This would then be a direct indication of the failure of the quenched approximation. Even so, one would expect that if an extrapolation is done from large enough masses it will extrapolate to zero at $m_f = 0$ indicating that the theory is in the high temperature phase.
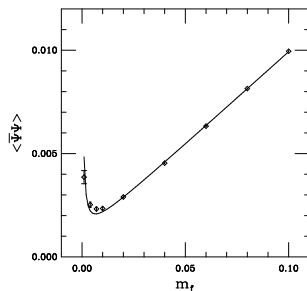
Figure 5. $< \overline{\Psi}\Psi >$ vs. m_f from a quenched QCD simulation above the transition. The lattice size is $16^3 \times 4$, $\beta = 5.71$, $L_s = 32$, and $m_0 = 1.9$.

In figure 5 the chiral condensate as a function of m_f is shown. The $1/m_f$ divergence for $m_f < 0.005$ is evident. The fit is to a form $c_{-1}/m_f + c_0 + c_1 m_f$. What is more surprising is that c_0 is not zero but $c_0 = 9.0(4)10^{-4}$. This is the first time such a phenomenon has been observed and is another indication of the failure of the quenched approximation (recently this was reproduced using different methods [21, 22]). This indicates that the remaining instantons, anti-instantons, in the absence of a fermion determinant, are capable in producing a non-zero density of small eigenvalues. Again, this is in sharp contrast with Wilson or staggered fermions.

6. QCD thermodynamics with DWF

In this section the parameter space of DWF for the two flavor QCD finite temperature transition is studied. This has appeared in [23, 24, 25, 27].

One would like to verify that DWF can be used in thermodynamic studies and to determine the range of the new parameters m_0 and L_s. A study of the full two flavor QCD on small lattices $8^3 \times 4$ is done in order to answer these questions.
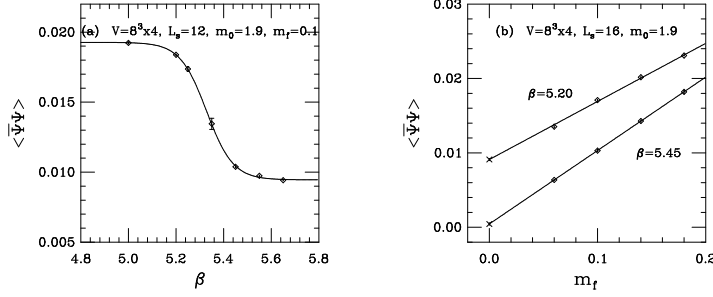
Figure 6. (a) $\langle \overline{\Psi}\Psi \rangle$ vs. β. (b) $\langle \overline{\Psi}\Psi \rangle$ vs. m_f below and above the transition.
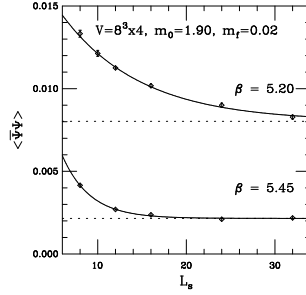
Figure 7. $< \overline{\Psi}\Psi >$ vs. L_s below and above the transition.

In figure 6a, for $m_f = 0.1$ and $L_s = 12$, one can clearly see a sharp crossover in the chiral condensate as β is varied. In figure 6b $\langle \overline{\Psi}\Psi \rangle$ is plotted vs. m_f for $L_s = 16$ at $\beta = 5.2$ below the transition and at $\beta = 5.45$ above the transition. Below the transition it extrapolates to a non zero value and above to a near zero value. In figure 7 $\langle \overline{\Psi}\Psi \rangle$ is plotted vs. L_s at $m_f = 0.02$. As can be seen, the decay is consistent to exponential. At $L_s = 24$ $\langle \overline{\Psi}\Psi \rangle$ has reached its asymptotic value above the transition while below the transition it is $\approx 10\%$ away. The dependence on m_0 has also been investigated [23, 25] and has been found that if m_0 is constrained in the region $1.6 < m_0 < 2.0$ then the theory has one flavor (in our case two, since we simulate with the square of the determinant of the Dirac operator). Below that region the light states disappear and above more flavors may be present.

Since DWF have explicit flavor symmetry, one can see that above the transition the full $SU(2) \times SU(2)$ chiral symmetry is present to a very good approximation at $L_s = 24$. Below the transition the symmetry is

spontaneously broken. For the first time the important symmetry properties of QCD at finite temperature are under control.

7. $U_A(1)$ Above the QCD finite temperature phase transition

The results from a study of the $U_A(1)$ symmetry just above the deconfinement transition are presented. This has appeared in [23, 24, 25, 26, 27].

As is well known the $U_A(1)$ axial symmetry of zero temperature QCD is broken by the anomaly. However, at finite temperature above the transition where the chiral symmetry is restored $U_A(1)$ may also be restored. This is an interesting subject because there are no experimental results relating to this yet and because the order of the transition may depend on it. Lattice simulations could contribute something important in this direction. Unfortunately, staggered fermions [28, 29] could not produce conclusive results because they do not have robust zero modes [29].
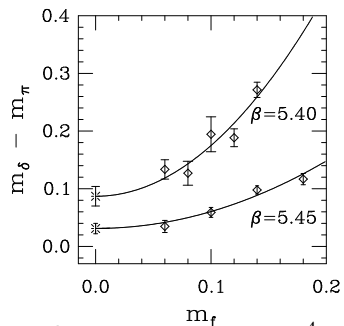

Figure 8. The δ minus the π mass on a $16^4 \times 4$ lattice for $L_s = 16$ and $m_0 = 1.9$. The fits are to $c_0 + c_2 m_f^2$ and the stars are the $m_f = 0$ extrapolated values.

On the other hand, DWF have exceptionally good zero mode properties as discussed in the previous sections. Therefore, they provide a powerful tool for such studies. The results from a large scale simulation of the full two flavor QCD on large volumes is presented in figure 8. The difference of the screening masses of the δ and π is used as a measure of anomalous symmetry breaking and is plotted vs. the bare quark mass m_f on a $16^3 \times 4$ lattice for $L_s = 16$ at $\beta = 5.45$ and $\beta = 5.40$ ($\beta_c \approx 5.325$). The lines are fits to $c_0 + c_2 m_f^2$ and have $\chi^2/\text{d.o.f.} \approx 1$. The fact that a linear term is not needed in order to give a good fit is an indication that for $L_s = 16$ the chiral symmetry is effectively restored (this can also be seen from figure 7). The $m_f = 0$ extrapolated values are 0.087(17) at $\beta = 5.40$ and 0.031(9) at $\beta = 5.45$. Although both are not zero by a statistically significant amount their value is small when compared with m_δ and m_π which are ≈ 1.3. Universality arguments require that if the QCD phase transition is to be

second order, the anomalous $U(1)_A$ must be broken. It is an open question as to whether the small size of the $U(1)_A$ symmetry breaking seen here is sufficient to support this theoretical prediction that the two-flavor QCD phase transition is second order [30].

8. The transition region of two flavor QCD

In this section a study of the transition region of two flavor full QCD is presented. This work has appeared in [25, 26, 31, 32]
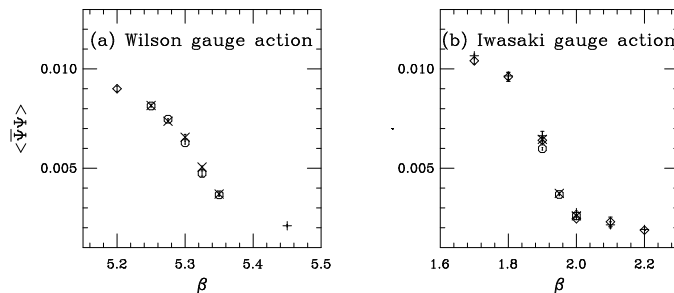
Figure 9. (a) $m_0 = 1.9$, $m_f = 0.02$ and $L_s = 24$. The circles correspond to $16^3 \times 4$ lattice with an ordered initial configuration (ic), the crosses to a $16^3 \times 4$ with disordered ic, the diamond to an $8^3 \times 4$ with ordered ic, and the plus to an $8^3 \times 4$ with disordered ic. The gauge part of the action is a Wilson plaquette action. (b) Same as in (a) but with an Iwasaki improved gauge action with $c_1 = -0.331$.

From the analysis in the previous sections it appears that DWF can reproduce the important physics of the deconfining transition. Also, the previous analysis indicates that $L_s = 24$, $m_f = 0.02$ and $m_0 = 1.9$ are reasonable settings for the new parameters. Armed with this knowledge a large scale numerical study of the transition region was done and the results are shown in figure 9a. The lattice size is $16^3 \times 4$ which corresponds to a physically relevant volume. The transition appears to be relatively smooth. In order to set the scale a zero temperature calculation was done at the transition coupling on an $8^3 \times 32$ lattice [31]. The scale was set using the ρ mass. The critical temperature was found to be $T_c = 163(4)$ MeV and the pion mass $m_\pi = 427(11)$ MeV. The critical temperature is in agreement with results obtained from other fermion regulators [33]. The pion mass is clearly too heavy. More sophisticated studies [18, 20] indicate that the residual chiral symmetry breaking effects are much larger than expected and in order to obtain a physical pion mass $L_s \approx 64 - 96$ may be needed.

On the other hand, one would expect that the use of a pure gauge action with better continuum limit properties may improve the chiral properties of DWF for the same L_s. The previous results were obtained using the

traditional Wilson plaquette action. A second large scale simulation was done using the Iwasaki improved pure gauge action with $c_1 = -0.331$ [34]. The results are shown in figure 9b. A similar scale setting calculation [31] at $\beta = 1.9$ gave $T_c = 166(3)$ MeV and $m_\pi = 400(7)$ MeV. The critical temperature is in agreement with the Wilson plaquette action but the pion mass did not get lighter by a significant amount.

The transition at these parameter values is clearly not first order. Simulations using ordered and disordered initial configurations at the transition point agreed after a few hundred iterations and did not show any signs of first order behavior. Therefore, one can conclude that the order of the two flavor QCD transition with three pions of mass ≈ 400MeV is not first order.

9. The transition region of three flavor QCD

Here the three flavor transition is discussed. This work is in progress [35].
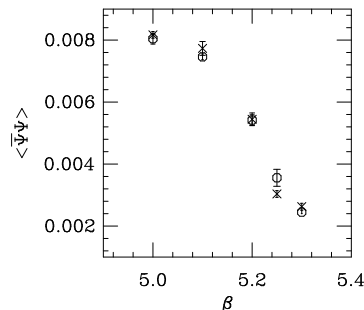
Figure 10. Three flavor QCD with Wilson plaquette action, $16^3 \times 4$, $m_0 = 1.9$, $m_f = 0.02$ and $L_s = 32$. The circles correspond to an ordered initial configuration and the crosses to a disordered one.

A very important question relates to the order of the finite temperature transition of QCD in nature. It is known that both Wilson and staggered fermions with three flavors produce a first order transition at small quark masses. However, they disagree on the values of the quark masses where this happens. Wilson fermions [36] predict a second order transition at physical quark masses while staggered fermions suggest a second order transition for the physical value of m_s and $m_d = m_u = 0$ and a cross-over for physical values of all three masses [37].

Because of the improved chiral properties of DWF it is hoped that significant progress can be made. The results of a preliminary study with three degenerate flavors with $L_s = 32$ and $m_f = 0.02$ are shown in figure 10. There is no evidence of a first order transition for these parameters. A simulation with $L_s = 64$ and $m_f = 0.01$ will begin shortly. In tandem, a similar calculation using staggered fermions is now in progress in order to

be able to directly compare the DWF results at some physical scale with those from staggered fermions at the same scale.

## 10. DWF improvements from the pure gauge sector

In this section improvements to the L_s behavior of DWF are discussed. The improvements are attempted by modifying the pure gauge part of the action. This work is in progress [35]. For other promising ideas see also [4, 5, 38].

As discussed in section 2, there appear to be two general sources that can slow down the approach to the chiral limit as L_s is increased. The first is due to fluctuations and the second is due to configurations in the vicinity of changing topology. As the continuum limit is approached both of those sources are suppressed. The first one since the continuum–like fields are "smoother" and the second one because different topological sectors are separated by increasingly large energy barriers that suppress topology changes. The problem is that thermodynamic calculations are necessarily restricted to relatively strong couplings since the available computing resources allow access to lattices with only a few lattice sites N_t along the time direction. For 2 flavor QCD with DWF and Wilson plaquette pure gauge action, the transition for $N_t = 4$ is at $\beta = 5.325$. As was seen in section 8, $L_s = 24$ is not enough to reduce the chiral breaking effects due to the regulator and as a result the pion mass is almost three times its physical value. It has been estimated that in order to bring the pion mass to physical values, $L_s = 64 - 96$ may be needed [18, 20]. Although this is possible with the 400 Gflops machine at Columbia University [39, 40], an improvement that will allow the same degree of chiral symmetry restoration for smaller L_s is very desirable. It is in this sense that improvements of DWF are discussed.

One could hope to improve DWF by improving the pure gauge part of the action so that the gauge field configurations will be "smoother" and will contain fewer objects that tend to change topology. The connection of DWF with the topology of the gauge field is pronounced and approximate forms of the index theorem on the lattice have been found [41] [12]. One could try to exploit this by manipulating the pure gauge sector and have a good chance that an improvement in the fermionic sector is achieved. This discussion is clearly heuristic and can only serve as a guide to the choice of actions. Once a choice has been made the effects can only be determined by explicit numerical simulations. In this spirit several actions have been examined.

10.1. IWASAKI ACTION FOR QUENCHED QCD AT $\beta = 5.7$

The Iwasaki pure gauge action is very appealing since it is expected to be closer to the continuum action. A quenched numerical simulation at $\beta = 5.7$ produced the m_π^2 values shown in figure 11. For comparison, the values with a Wilson plaquette action are also shown. Both sets are the extrapolated $m_f = 0$ values. The Iwasaki points at $L_s = 16$ are lower than the Wilson points at $L_s = 48$! This indicates that at these lattice spacings ($a^{-1} \approx 1$ GeV) an important improvement has been found.
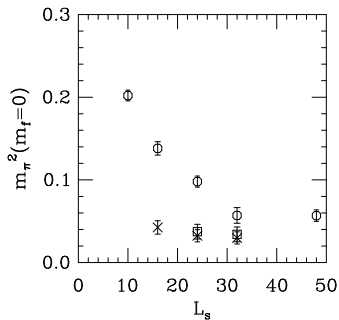
Figure 11. m_π^2 extrapolated to $m_f = 0$ vs. L_s. The circles are for the Wilson plaquette action and with $m_0 = 1.9$. The crosses are for the Iwasaki action with $m_0 = 1.65$ and the squares with $m_0 = 1.9$

10.2. WILSON PLAQUETTE ACTION

In what follows the Wilson single plaquette action with dynamical 2 flavor DWF is used as a "benchmark". Since dynamical simulations are very demanding small lattices with size $8^3 \times 4$ are used at $L_s = 24$, $m_f = 0.02$, $m_0 = 1.9$ in order to locate the transition. Then a zero temperature simulation is done on an 8^4 lattice at the critical coupling in order to measure m_{res}. This measurement is possible due to the work in [18, 20]. Here the more naive $m_{\text{res}} = \langle \overline{\Psi}\Psi \rangle / \chi_\pi - m_f$ is used. Since we are looking for improvements by a factor of two or larger this naive estimation is adequate. The transition is at $\beta_c = 5.325$, where $m_{\text{res}} = 0.028(2)$ and $a^{-1} \approx 700$ MeV.

10.3. IWASAKI ACTION

From the success at $a^{-1} \approx 1$ GeV of the quenched theory one could reasonably expect that a similar effect will be present in dynamical QCD near the transition. Unfortunately, as already observed in section 8, this is not the case since the pion mass is about the same. Also, a measurement of m_{res} at the transition ($\beta_c = 1.9$) produced $m_{\text{res}} = 0.030(3)$ which is similar to

the Wilson case. This failure to improve could be due to the larger lattice spacing at β_c ($a^{-1} \approx 700$ MeV) as compared to $\beta = 5.7$ quenched.

10.4. THE RESTRICTED PLAQUETTE ACTION

It has been found that small size objects are responsible for most of the "unphysical" topology changes [12]. One would expect such objects to be associated with larger than normal plaquette values. Therefore, one could restrict the value of $1 - Tr[U_p]/3$ to be less than a certain value and hope to reduce the presence of such objects. A histogram of $1 - Tr[U_p]/3$ for the Wilson action with dynamical DWF just below the transition is shown in figure 12a. An action with a term $([1 - Tr[U_p]/3]/c)^{20}$ suppresses values of $1 - Tr[U_p]/3$ above the cutoff "c". For $c = 0.8$ it was found that $\beta_c \approx 1.4$ and $m_{\mathrm{res}} = 0.027(1)$. For $c = 0.75$, β_c was less than 0.01 and it did not make sense to pursue further. Obviously there is no improvement. However, the dependence of β_c on "c" is surprising since $c = 0.75$ is still in the tail of the distribution in figure 12a. The distribution for $c = 0.8$ is in fig. 12b.
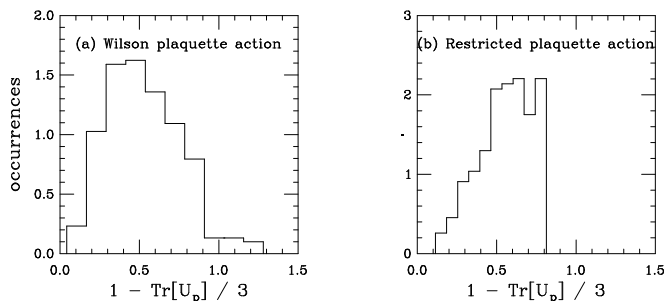
Figure 12. Histogram of $1 - Tr[U_P]/3$. The area under the curve is normalized to one. The lattice size is $8^3 \times 4$, $L_s = 24$, $m_f = 0.02$ and $m_0 = 1.9$. (a) Wilson plaquette action at $\beta = 5.275$. (b) restricted plaquette action with $c = 0.8$ at $\beta = 1.2$. Both are just below the transition.

10.5. THE ENHANCED RECTANGLE ACTION

At large N_t one could imagine that the transition is driven by instanton type objects of many sizes. Then removing the objects of size one and less would not affect the transition and may improve DWF. But at $N_t = 4$ one could imagine that only objects of size one and two exist. Distinguishing them could be very hard. To test these ideas the following action that enhances objects with size ≈ 2 through the transition by a fixed amount was used:

$$\beta \frac{Tr[U_p]}{3} - x \frac{Tr[U_r]}{3} \quad , \tag{3}$$

where U_r is the product of links around the 1×2 rectangles. This action has the correct continuum limit since the second term is of order g^2. The difference from the Iwasaki action is that the rectangle has a β independent coefficient $x = 3.0$. The transition is at $\beta \approx 15$. At that coupling $m_{\rm res} = 0.0050(4)$! This large improvement lends support to the above speculations.

Furthermore, it provides us with another picture [42]. As is known for the Iwasaki action if a large instanton begins to shrink it will encounter an energy barrier and will not be able to shrink below one to two lattice spacings. These ideas were developed in relation to the cooling methods but they are clearly relevant here. These energy barriers may make it more difficult for instanton-like objects to shrink below the lattice spacing and therefore change topology. This could be an alternative explanation for the improvement seen with Iwasaki action at quenched $\beta = 5.7$ ($a^{-1} \approx 1$ GeV). Also, since it is known that the more negative the coefficient of the rectangle the larger the barrier, the observed improvement with the action of eq. 3 at $a^{-1} \approx 700$ MeV is not unexpected. Currently, an Iwasaki type action with $c = -1.0$ as in [43] is being investigated [35].

11. DWF improvements from the fermion sector

Other improvements can be attempted by changes in the fermion sector.

As discussed earlier, the topology changing configurations are the ones for which the transfer matrix has a unit eigenvalue. It is known that this is equivalent with the traditional Wilson Dirac operator with mass equal to $-m_0$ having a zero eigenvalue [11, 8]. Therefore, including extra species of Wilson fermions with Dirac operator $D^\dagger D + h^2$ may reduce these eigenvalues depending on the value of the parameter h. This work is in progress [35].

Acknowledgments

References

1. D.B. Kaplan, Phys. Lett. B 288 (1992) 342.
2. D.B. Kaplan, Nucl. Phys. B (Proc. Suppl.) **30** (1993) 597.
3. R. Narayanan, Nucl. Phys. **B34** (Proc. Suppl.) (1994) 95; M. Creutz, Nucl. Phys. **B42** (Proc. Suppl.) (1995) 56; Y. Shamir, Nucl. Phys. **B47** (Proc. Suppl.) (1996) 212; T. Blum, Nucl. Phys. **B73** (Proc. Suppl.) (1999) 167; H. Neuberger, Lattice 99 proceedings, hep-lat/9909042; M. Lüscher, Lattice 99 proceedings, hep-lat/9909150;

4. H. Neuberger, these proceedings, hep-lat/9912013.
5. Y. Shamir, these proceedings, hep-lat/9912027.
6. These proceedings: W. Bietenholz, hep-lat/0001001; A. Borici, hep-lat/9912040; M. Creutz, hep-lat/9912006; U. Heller, hep-lat/9912043, hep-lat/9912042; I. Horvath, hep-lat/9912030; W. Kerler; A.A. Slavnov; M. Wingate.
7. Y. Shamir, Nucl. Phys. B **406** (1993) 90.
8. V. Furman, Y. Shamir, Nucl. Phys. **B439** (1995) 54.
9. P.M. Vranas, Lattice 96, Nucl. Phys. **B53** (Proc. Suppl.) (1997) 278; Phys. Rev. **D57** (1998) 1415.
10. R. Narayanan, H. Neuberger, Phys. Lett. B **302** (1993) 62.
11. R. Narayanan, H. Neuberger, Phys. Rev. Lett. **71** (1993) 3251; Nucl. Phys. B **412** (1994) 574; Nucl. Phys. B **443** (1995) 305.
12. U.M. Heller, R. Edwards and R. Narayanan, Nucl. Phys. **B535** (1998) 403; Phys.Rev. D60 (1999) 034502.
13. R. Narayanan, H. Neuberger and P. Vranas, Phys. Lett. B **353** (1995) 507; Nucl. Phys. B (Proc. Suppl.) **47** (1996) 596.
14. P.M. Vranas, I. Tziligakis and J. Kogut, to appear in Phys. Rev. **D**, hep-lat/9905018.
15. S. Aoki, Phys. Rev. **D30** (1984) 2653; S. Aoki, S. Boettcher and A. Gocksch, Phys. Lett. **B331** (1994) 157.
16. S. Aoki, Lattice 99 proceedings, hep-lat/9909154.
17. P. Chen et.al., Phys. Rev. **D59** (1999) 054508.
18. G. Fleming et.al., Nucl. Phys. **B73** (Proc. Suppl.) (1999) 207.
19. A. Kaehler et.al., Nucl. Phys. **B73** (Proc. Suppl.) (1999) 405.
20. G. Fleming, Lattice 99 proceedings, hep-lat/9909140.
21. R. Edwards, U. Heller, J. Kiskis, and R. Narayanan, hep-lat/9910041.
22. J.F. Lagae and D.K. Sinclair, Lattice 99 proceedings, hep-lat/9909097.
23. P.M. Vranas et.al., Nucl. Phys. **B73** (Proc. Suppl.) (1999) 456.
24. N. Christ et.al., contribution to ICHEP 98, hep-lat/9812011.
25. P.M. Vranas, contribution to DPF 99 proc., UCLA, hep-lat/9903024.
26. P.M. Vranas, Lattice 99 proceedings, hep-lat/9911002.
27. G. Fleming, contribution to PANIC 99, Uppsala, Sweden, hep-ph/9910453.
28. S. Chandrasekharan, D. Chen, N.H. Christ, W. Lee, R. Mawhinney, and P.M. Vranas, Phys. Rev. Lett. **82** (1999) 2463.
29. J.B. Kogut, J.F. Lagae, D. K. Sinclair, hep-lat/9801020.
30. R. Pizarski and F. Wilczek, Phys. Rev. **D29** (1984) 338.
31. L. Wu, Lattice 99 proceedings, hep-lat/9909117.
32. R. Mawhinney, Lattice 99 proceedings.
33. F. Karsch, Lattice 99 proceedings, hep-lat/9909006.
34. Y. Iwasaki, Nucl. Phys. B **258** (1985) 141.
35. In progress, P. Chen, N. Christ, C. Cristian, G. Fleming, A. Kaehler, T. Klassen, X. Liao, G. Liu, C. Malureanu, R. Mawhinney, G. Siegert, C. Sui, L. Wu, and Y. Zhestkov.
36. Y. Iwasaki et.al., Phys. Rev. **D54** (1996) 7010.
37. F. Brown et.al, Phys. Rev. Lett. **65** (1990) 2491.
38. H. Neuberger, hep-lat/9911004.
39. N. Christ, et.al. Nucl. Phys. **B73** (Proc. Suppl.) (1998).
40. N. Christ, Lattice 99 proceedings, hep-lat/9912009.
41. R. Narayanan, P. Vranas, Nucl. Phys. **B506** (1997) 373.
42. I am grateful to P. van Baal, T. Kovacs and I. Stamatescu for pointing this out to me.
43. Y. Iwasaki and T. Yoshiè, Phys. Lett. **B131** (1983) 159.